Three-Dimensional Study of Inclusion Morphology and Size Distribution In Mn-Si Killed Steel

Obinna M. Adaba*, Ronald J. O'Malley, Mingzhi Xu, Laura N. Bartlett, Simon N. Lekakh

Missouri University of Science and Technology
Materials Science & Engineering Dept.
1400 N Bishop
Rolla, MO 65409

*Presenting and corresponding author
omakc2@mst.edu
(573) 341-7683

ABSTRACT

Inclusion size distribution and shape are typically determined from the analysis of a polished cross-section of steel specimen. However, measured inclusion characteristics such as 2D size distribution can differ from the actual 3D characteristics that influence the mechanical properties of steel. In this study, $MnO{\cdot}SiO_2$ inclusions that were liquid at steelmaking temperatures have been extracted from a Mn-Si killed steel using an electrochemical dissolution method to reveal the actual 3D size distribution and shape. Automated SEM/EDX analysis was used to perform a direct comparison of the inclusions observed in 2D polished section and in 3D by analyzing extracted inclusions collected on a filter. A spherical inclusion shape was assumed and used to perform the statistical conversion of measured 2D particles to a virtual 3D particle size distribution and the predicted distribution was compared to the measured 3D distribution. The causes of the departure of the real 3D inclusion statistics from the converted 2D data are discussed.

INTRODUCTION

Proper characterization of non-metallic inclusions in steel is crucial in understanding their effect on steel quality and the mechanical properties of the as-cast product [1, 2, 3]. Knowledge of how the inclusion size, composition, and morphology changes for different steelmaking practices also helps in process optimization and in engineering the inclusion characteristics to meet specific steel property and performance requirements.

Inclusion analysis is typically performed on polished 2D cross sections and relevant information about their characteristics are drawn from these results. These results however, are subject to errors which vary depending on the complexity of the inclusion shape and statistical quantification method that is employed. Even for the simple case of a distribution of ideal random spherical particles in a volume, the results of a 2D cross section analysis depends on the chosen sample plane of analysis, the critical number of inclusions counted, the assumed maximum particle size and other parameters [4]. Figure 1a shows a simplified example for an inclusion population with uniform diameter spherical particles distributed in a cube. The cube is sectioned midway through its height to reveal the 2D circular cross section of inclusions that are intersected by the plane, Figure 1b. For a large sample size, the probability distribution of the 2D circle diameters that

intersect with the sample plane is shown in Figure 1c. While the original particles were spheres with the same diameter, the 2D sections produce circles with different sizes that are observed in accordance with the probability distribution. The interpretation of the 2D data becomes even more complicated for random distribution of spheres with different diameters and a shape departure from that of ideal spheres.

Different statistical techniques are available for transforming the size distribution of particles observed on 2D cross sections to their actual distributions by assuming ideal spheres or ellipsoidal shapes [4, 5]. The most common method is the Schwartz-Saltykov method for area analysis, which is applicable to particles of different shapes as long as the shape probabilities are known. This method groups particles by their areas into lognormal class sizes where each smaller class size is less than the next larger class size by a factor of $10^{\wedge -0.2}$. This method also assumes that the maximum 3D particle size equals the observed maximum 2D size. Application of this method to non-metallic inclusions was simulated by T. Li et al [6] and reasonable agreements were observed between the transformed 2D and the actual inclusion size distribution. These results however, were based on averaging 2D cross section results for at least 30 different cross sections, which is impractical. Also, the effect of the transformation when the inclusions are not spherical were not discussed.

In this study, $MnO{\cdot}SiO_2$ inclusions with a simple spherical shape were studied. These inclusions were characterized on both 2D polished cross sections and on the filter paper after extraction to reveal their actual size, and morphology. Analysis was done using an SEM/EDX system with automated feature analysis capability (ASPEX). The Schwartz-Saltykov statistical method was used for converting 2D to 3D and the actual and predicted particle size distributions were compared.

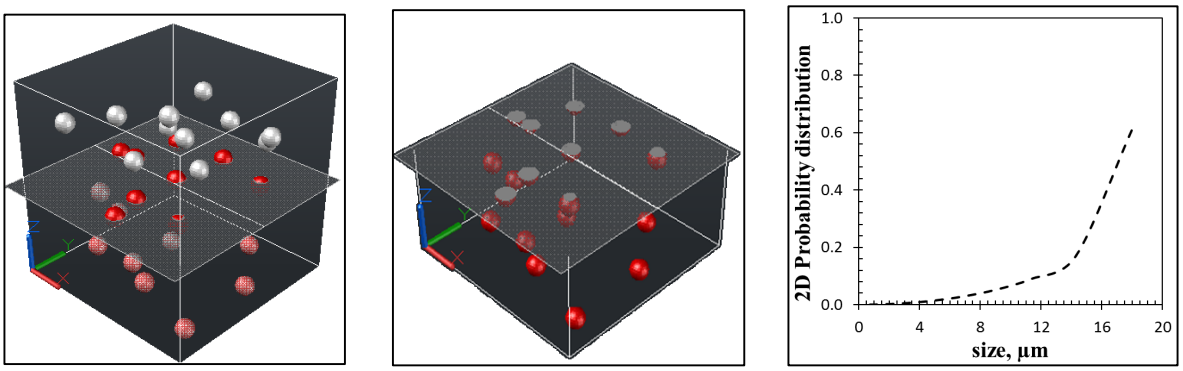

(a) (b) (c)

Figure 1: (a) Particle distribution in 3D, (b) circles on the 2D section and (c) relative probability of observed circle diameters for a mono-sized sphere population.

EXPERIMENTAL PROCEDURE

Liquid steel deoxidation experiments were performed in a 100 lbs. induction furnace. High purity induction iron and 0.2wt.% of pure graphite were charged and melted under argon protection. Table 1 shows the composition of the steel melt. Once the temperature of the melt had reached 1600^{0}C, samples for inclusion analysis were taken with a specially constructed 38mm diameter

submerged zirconia ceramic shell sampler. Manganese and silicon additions were placed in each sampler (Figure 2a) to kill the steel and produce $MnO{\cdot}SiO_2$ inclusions when it was dipped into a melt with a controlled total oxygen content. Samplers were held at different times, withdrawn, and then quenched in a water bath to investigate the early stages of inclusion formation in the sampler. The holding times employed in this experiment were 0, 1, and 2 minutes and the mass of ferro-alloys added to the sampler were 1g FeSi, and 2.25g FeMn, respectively, into approximately 224g of liquid steel in the sampler. Figure 2b shows the thermodynamically predicted composition of the deoxidation products calculated using Factsage 7.1 using the FactPS, FTMisc, and FToxid databases.

Table 1. Composition of liquid steel.

Element	C	Mn	Si	S	Al
Amount, wt.%	0.2	0.03	0.003	0.003	0.001

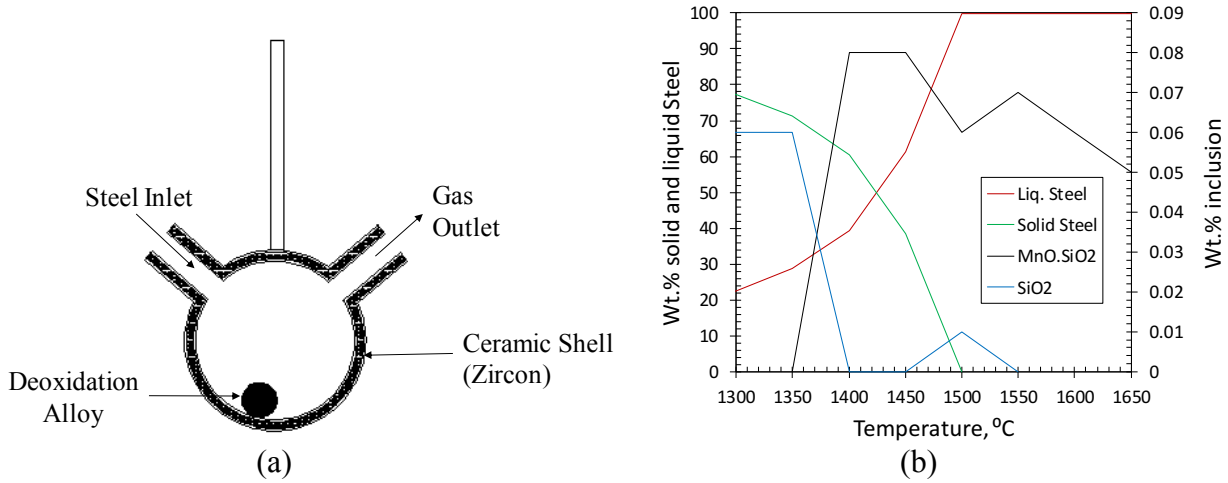

Figure 2: (a) Ceramic shell liquid steel sampler and (b). Factsage predicted reaction products. At 1600^0C and the targeted steel composition, $MnO{\cdot}SiO_2$ inclusions are shown to be in equilibrium with the steel

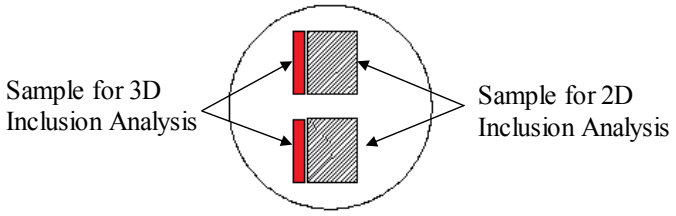

Figure 3: Cross section of the sampler showing specimen locations for 2D and 3D inclusion analysis.

After the experiment, the samplers containing the steel samples were sectioned at a distance which was one-third from the sample base and steel section samples taken for both 2D and 3D inclusion analysis (Figure 3). Two samples were taken for each test. The 2D sectioned samples were ground and polished to a 1µm surface finish using diamond paste while samples for 3D inclusion analysis were ground, cleaned in an ultrasonic bath and the steel was then dissolved in an electrolytic cell using the steel as the anode and platinum as the cathode. The composition of the solution used for

electrolytic dissolution was similar to that described by the authors [7, 8]. The solution was composed of 2v/v% triethanolamine and 1w/v% tetramethyl ammonium chloride methanol solution. For all steel dissolution experiments, the anode current density was set to between 40-60mA/cm^2 and the amount of steel dissolved varied from 0.2g to 0.5g. After extraction, the solution was filtered through a 0.05µm polycarbonate filter and the filter paper containing the inclusions were gold coated for SEM analysis.

The characteristics of the inclusions on the 2D cross section and on the filter paper after extraction were determined using an automated feature analysis (AFA) in the Aspex Pica 1020 SEM with EDX analysis. The minimum inclusion size for the SEM-AFA analysis was 0.5µm and the analysis was done at a magnification of 1000x and a step size of 0.31µm. For each analysis, the minimum number of inclusions counted was about 4500.

RESULTS AND DISCUSSION

$MnO{\cdot}SiO_2$ Inclusion Composition and Shape

Deoxidation experiments with the manganese and silicon placed in the sampler before dipping into the steel produced $MnO{\cdot}SiO_2$ inclusions. These inclusions are known to be liquid at steelmaking temperatures of 1600°C, and thus, have a near spherical shape. Figure 4a shows a $MnO{\cdot}SiO_2$ inclusion on a 2D cross section and figure 4b shows an inclusion after it had been extracted from the steel. On the 2D cross section, the inclusion appears circular and corresponding spherical inclusions were observed after extraction. The comparisons between the average inclusion compositions obtained after the AFA analysis is shown in Figure 5. These plots were generated by considering the 3 elements which have the highest percentages in each counted inclusion and normalizing with respect to them. Each ternary therefore represents distinct $MnO{\cdot}SiO_2$ inclusions with the third highest concentration elements being aluminum or sulfur. Also, the liquid phase region (outlined by yellow) at 1600°C is shown on these plots. This region was calculated using Factsage 7.1 and with the FactPS, FTMisc, and FToxid databases. It can be seen from both figures that most of the inclusions are within the liquid phase and that both the 2D and 3D inclusions analysis have similar compositional distributions. Table 2 shows the average inclusion wt. percentages from both methods. Similarities in the composition of the 2D and 3D inclusions provide supporting evidence that the extraction process did not alter 3D the inclusion population.

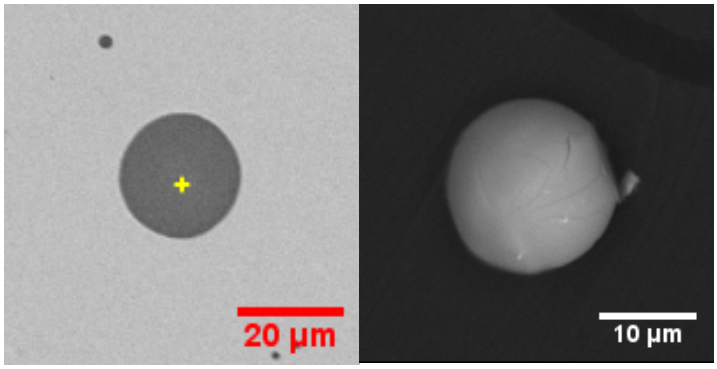

(a) (b)

Figure 4: Shape of $MnO{\cdot}SiO_2$ inclusions on (a) 2D cross section and (b) after extraction from the steel (3D). Circular inclusions on the 2D cross section are shown to be spherical after extraction.

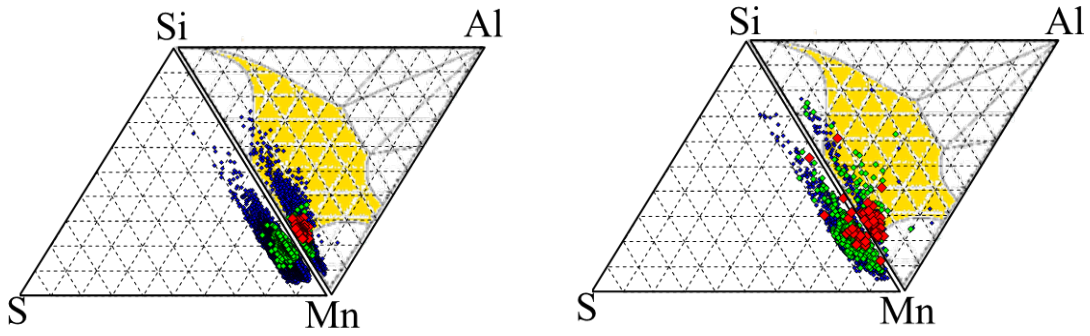

Figure 5: Composition of the $MnO{\cdot}SiO_2$ inclusion obtained from (a) 2D cross section analysis and (b). After extraction from the steel. Compositions are similar for both methods.

Table 2. Average inclusion composition, wt.%.

Method	Al	Si	S	Mn
2D Analysis	2	20	2	75
3D Analysis	2	24	3	71

Size Distribution of $MnO{\cdot}SiO_2$ Inclusions

Two types of quantitative analysis were performed using the SEM-AFA data. The first compared the area fraction (AF) of inclusions on the cross section with the volume fraction (VF) of extracted inclusion from dissolution. The second compared the 2D and 3D size distributions. The AF was calculated by dividing the total area of the counted inclusions on the 2D cross section by the scan area while the VF was calculated by dividing the total inclusion volume by the volume of steel dissolved. The inclusion volume was calculated assuming the extracted inclusions to be perfect spheres and the volume of steel dissolved was determined according to equation 1.

$$\textbf{Volume dissolved} = \frac{\textbf{Area of filter scanned } (\textbf{mm}^2)}{\textbf{Total Filter area } (\textbf{mm}^2)} \textbf{ x } \frac{\textbf{Steel mass dissolved (g)}}{\textbf{Steel density } (\frac{0.0078\textbf{g}}{\textbf{mm}^3})} \qquad \textbf{(1)}$$

The calculated AF and VF were in poor agreement, suggesting that a portion of the extracted inclusions were not being counted. Possible reasons for this difference are a non-uniform distribution of the inclusions on the filter paper or partial losses of inclusions during extraction and filtering process. Additional tests were performed to assess the possible source of the discrepancy In the first investigation, two areas on the filter paper were selected and the inclusions within these areas analyzed (Figure 6). From this test, the detected inclusion numbers and size distributions in these two areas were similar. This suggests that inhomogeneity in particle distribution on the filter cannot account for the discrepancy. In the second investigation, a different filter paper with a finer pore structure was used during extraction. In this case, more fine inclusions (<0.5 microns) were observed on the filter surface, suggesting that the first filter paper did not capture all of the extracted inclusions. In future studies, the filter paper type and the steel volume used for extraction will be optimized to improve inclusion capture and analysis.

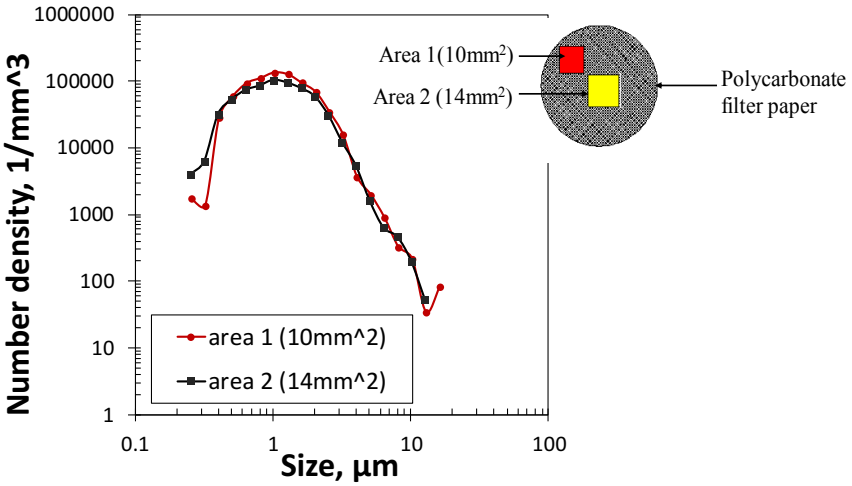

Figure 6: Comparison of size distribution of counted inclusions in two different selected areas on the filter paper, shown on insert. Homogeneous distribution of inclusions on the filter paper is observed

The second type of quantitative inclusion analysis was a comparison of 2D and 3D particle size distributions from the two characterization methods. For this comparison, it was assumed that the particle losses during filtration had a minimal influence on the inclusion size distribution with diameters larger than 0.5µm. Graphs in figure 7 show the size distribution of the inclusions on the 2D cross section and corresponding inclusions after extraction. The respective 2D and 3D inclusion number densities have been normalized with respect to their total number densities and the results are shown for samples 1, 2, and 3 which were taken 0, 1, and 2 minutes after deoxidation respectively. Plots were generated by binning the inclusion areas according to the method described by Schwartz-Saltykov [5] and counting the relative number of inclusions in each bin size.

For all samples, the distribution on the 2D cross section is observed to be shifted towards smaller inclusion sizes. This observed difference can be explained by the 2D sectioning statistics of a 3D inclusion population, which produces smaller observed diameters on the 2D plane. A summary of all of the analyzed data is shown in Table 3 and the results indicate that the mean 3D inclusion size is greater than the mean 2D size by approximately 22%.
Also worth pointing out is that the inclusion distribution from both the cross section and extracted inclusion analyses are lognormal in shape and thus have a similar quadratic shape on a log-log plot. Figures 8a and 8b are lognormal distribution fits for the 2D and corresponding 3D data in sample 3 and figure 8c shows the distributions on a log-log scale. Distribution fit tests were done with Minitab and for all samples, the lognormal distribution was found to be the best fit. A deviation from linearity at around 0.5µm can seen in both plots This deviation is a result of the size detection limit of the Aspex AFA analysis, which is 0.5µm. This preservation of distribution shape is important as recent studies [9, 10] have shown that the distribution shape is relevant in understanding physiochemical inclusion changes that occur during steel processing. In particular, newly formed inclusion populations have been shown to exhibit a lognormal distribution, while aged populations take on a power law distribution (linear on a log-log plot). The results presented here suggest that 2D data can be used effectively to evaluate the inclusion population age without the need to convert the population to 3D.

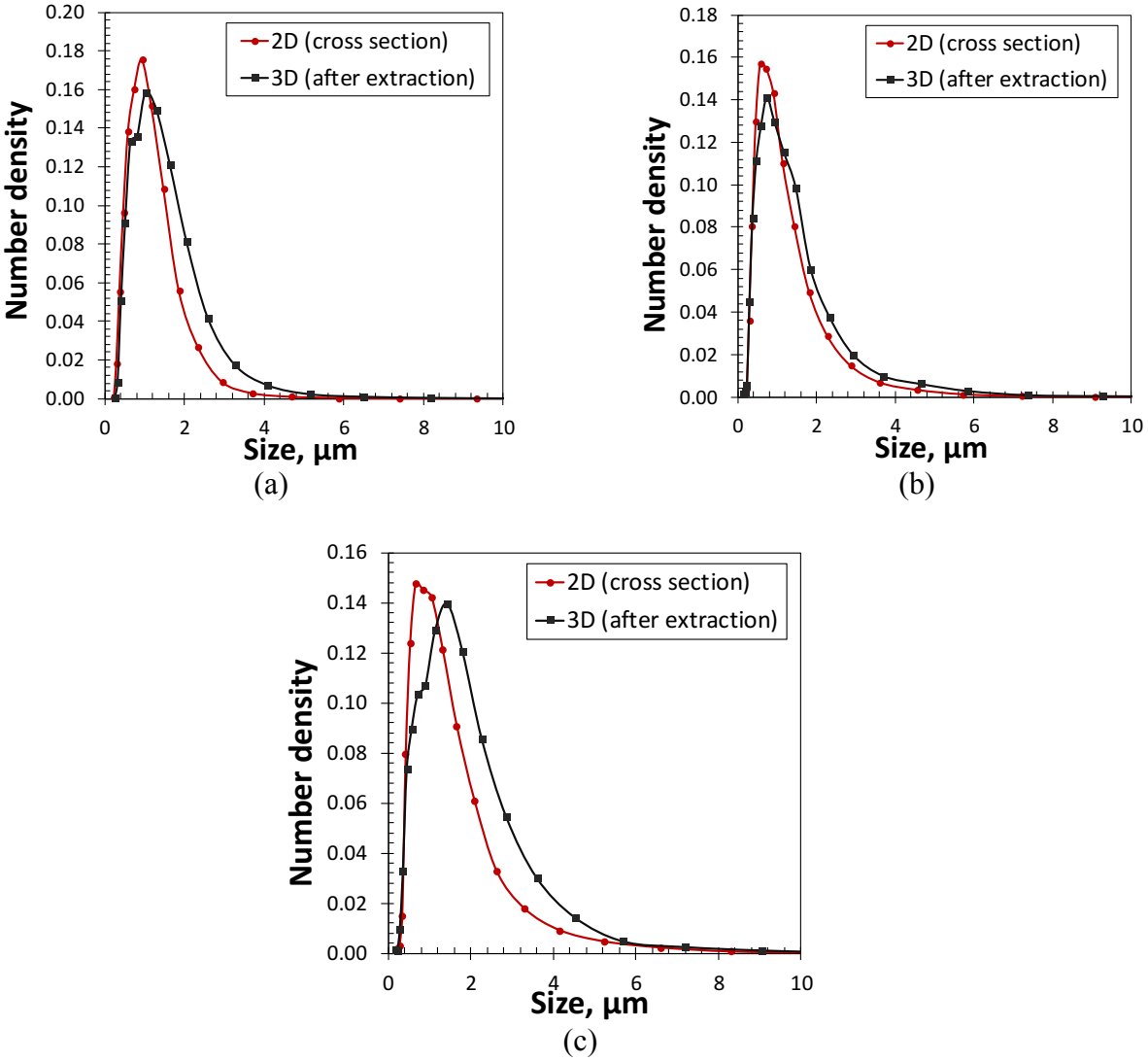

Figure 7: Size distribution of $MnO{\cdot}SiO_2$ inclusions on 2D cross section and after extraction: for (a) sample 1, (b) sample 2, (c) sample 3. Samples were taken at 0, 1, and 2mins after deoxidation. Plots show a distribution fit towards smaller inclusion sizes on the 2D cross section.

Table 3: Summary of results of automated SEM/EDX inclusion analysis from the 2D cross section and after extraction (3D).

Sample/time after deoxidation	Method	Average Inclusion Size (µm)	Maximum Inclusion Size (µm)
Sample 1/0 min	2D	1.2	23.4
	3D	1.6	13.0
Sample 2/1 min	2D	1.4	18.1
	3D	1.9	18.5
Sample 3/2 min	2D	1.6	20.8
	3D	2.0	33.5

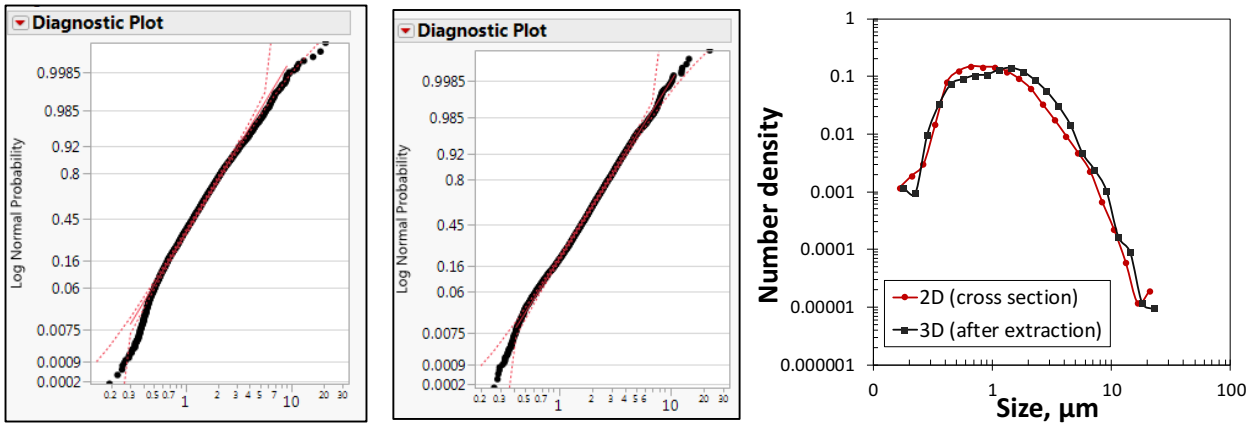

(a) (b) (c)

Figure 8: Lognormal fit test of the $MnO{\cdot}SiO_2$ inclusion obtained from (a) 2D cross section analysis and (b). After extraction from the steel. The horizontal axis represents inclusion size in microns and a deviation at 0.5µm is observed in both plots and is due to the detection limit of the machine. On a log-log scale, both distributions are observed to be quadratic. Hence, a preservation of distribution shape in both 2D and 3D

Application of Schwartz-Saltykov Method for 2D to 3D Transformation of Non-Metallic Inclusion in Mn-Si Killed Steel

The Schwartz-Saltykov method requires that the number of inclusions per unit volume of the largest inclusion size first be statistically determined from its number per area on the cross section. Once this is known, the portion of this largest inclusion size which is present in the relatively smaller cross section inclusion densities are calculated based on the probability distribution for the particular inclusion shape. These determined portions are then subtracted from the observed cross section number densities of smaller inclusions and the steps repeated until all portions of larger inclusion in the smaller sizes are determined and subtracted. The number per unit volume (N_V) is determined according to Eq. 2 where N_A is the observed cross section number per area, and P is the probability of finding N_A with diameter D. For spherical particles, this probability distribution is well known and is shown by Eq. 3. Where "D" is the maximum particle size and d_1 and d_2 are the lower and upper bin width sizes. One advantage of using the Schwartz-Saltykov method for area analysis is that it divides the inclusion areas and diameters into lognormal bin widths. By doing this, the probability distribution remains the same for all inclusion sizes and thus speeds up the calculations. Possible sources of error though are in the assumption of the maximum inclusion size as that observed on the cross section, the number of inclusions detected for this maximum inclusion size, and also using the right probability distribution.

$$N_V = \frac{N_A}{P * D} \tag{2}$$

$$P(d_1 < d < d_2) = \frac{1}{D}\left(\sqrt{D^2 - d_1^2} - \sqrt{D^2 - d_2^2}\right) \tag{3}$$

The result from the application of this method to the cross section data of sample 3 is shown in figure 9a. This result shows some discrepancies between the calculated 3D distribution and the measured 3D distribution from the analysis of extracted inclusions. The predicted distribution is shifted towards smaller inclusion sizes rather than towards larger inclusion sizes as experimentally observed in the extracted inclusion distribution. The results of the recalculated numbers per area and numbers per volume are shown in table 4. From this table, it can be seen that for the smallest inclusion sizes, the recalculated number densities are negative. Only a small number of inclusions were counted in the largest and smallest inclusion sizes of the 2D cross section. The resulting negative number densities of the smaller inclusion sizes and error in the predicted distribution are therefore, possibly due to a propagated error from subtracting portions of larger inclusion sizes, the size detection limit of the Aspex and small number of counted inclusions which are less than 0.5µm, and also the assumed maximum inclusion size.

With a greater number of inclusions counted in the maximum class size, the statistically determined portions of this inclusion size in smaller class sizes would be greater and hence, the subtractions would produce smaller numbers and shift the curve downwards. While this might match the observed 3D distribution eventually, it seems unlikely that this accounted for the observed errors. The predicted distribution was replotted by making an assumption that the maximum inclusion size is larger than the size observed in the 2D section. Plots were generated for different maximum sizes and figure 9b shows the predicted distribution when the maximum size is assumed to be 50% greater than the observed maximum size on the 2D cross section. By making this assumption, the curve is observed to shift towards the right and fit the distribution of the extracted inclusions up until a certain size of about 1µm. If all inclusions were correctly accounted for during analysis of inclusions on the filter paper, this result suggests that the basic underlying assumption on the maximum inclusion size and the detection limit of the Aspex produced the errors. To correctly determine what the maximum inclusion size should be, dissolution tests are being redone using the new filter paper with the aim of capturing and analyzing all inclusions on the filter paper.

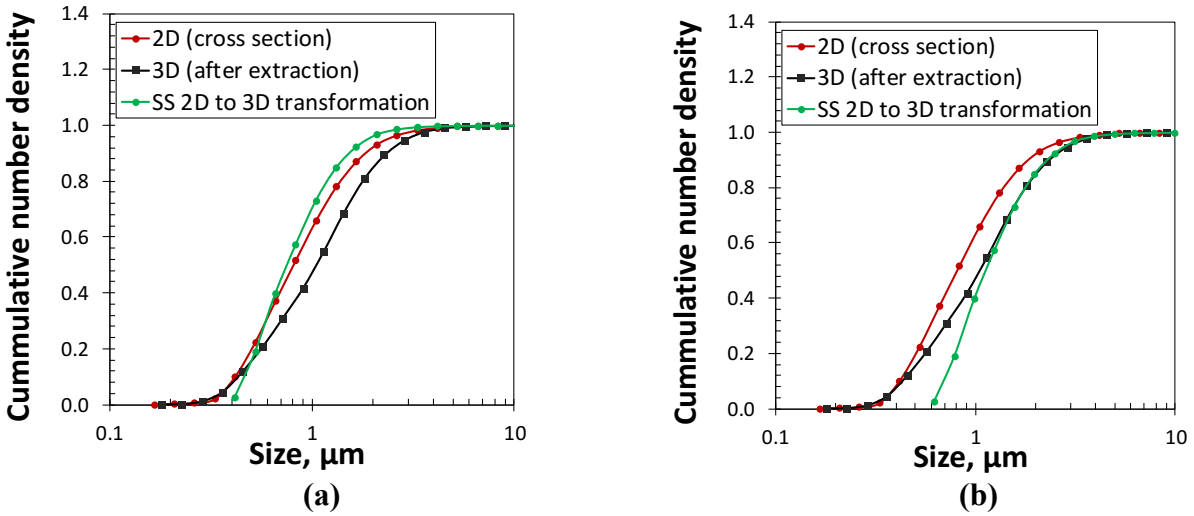

Figure 9; Comparison of the 3D transformed distribution obtained from the Schwartz-Saltykov method with experimentally measured 2D cross section and extracted inclusions (a) Assuming max. 2D size is same as 3D size, and (b) Max. 3D size is 50% greater than observed 2D size. A better distribution fit is observed by making this assumption of maximum inclusion size

Table 4: 2D and recalculated 3D results after application of the Schwartz-Saltykov method: Negative numbers are observed for small inclusion sizes

2D						3D	
Upper class dia. (µm)	Lower class dia. (µm)	Probability	bin width (µm)	Inclusion count	2D Number per area ($1/mm^2$)	Recalculated 2D number per area ($1/mm^2$)	Calculated 3D Number per volume ($1/mm^3$)
20.82	16.54	0.607	4.28	2	0.066	0.066	5.188
16.54	13.14	0.168	3.40	1	0.033	0.015	1.456
13.14	10.43	0.090	2.70	4	0.131	0.118	14.73
10.43	8.29	0.052	2.15	12	0.394	0.353	55.75
8.29	6.58	0.031	1.70	29	0.951	0.832	165.15
6.58	5.23	0.019	1.35	77	2.526	2.231	557.8
5.23	4.15	0.012	1.08	126	4.134	3.355	1056
4.15	3.30	0.007	0.85	195	6.397	5.045	1999
3.30	2.62	0.005	0.68	301	9.875	7.735	3859
2.62	2.08	0.003	0.54	441	14.47	11.14	6999
2.08	1.65	0.002	0.43	653	21.42	16.50	13045
1.65	1.31	0.001	0.34	771	25.29	17.99	17912
1.31	1.04	0.0007	0.27	818	26.84	17.80	22311
1.04	0.83	0.0005	0.21	762	24.99	15.02	23694
0.83	0.66	0.0003	0.17	618	20.28	10.49	20836
0.66	0.52	0.0002	0.14	499	16.37	7.897	19745
0.52	0.42	0.0001	0.11	333	10.93	3.855	12133
0.42	0.33	7.347 E-5	0.09	170	5.577	0.403	1595
0.33	0.26	4.635 E-5	0.07	25	0.820	-2.345	-11699
0.26	0.21	2.625 E-5	0.05	4	0.131	-1.140	-7161
0.21	0.17	1.845 E-5	0.04	2	0.066	-0.459	-3633
0.17	0.13	1.164 E-5	0.03	1	0.033	-0.210	-2095

CONCLUSION

The shape, composition, and size distribution of $MnO{\cdot}SiO_2$ inclusions on a 2D cross section were compared to the corresponding 3D size distribution after dissolving the steel and analyzing the extracted inclusions using the same automated SEM/EDX analysis system. The Schwartz-Saltykov method for transforming 2D data to 3D was applied and comparisons made between the measured and predicted 3D distributions. The results from these comparisons showed:

- Similar inclusion compositions were observed between the analysis of the polished 2D cross section of inclusions and the extracted inclusions using EDX analysis, suggesting that the extraction process did not alter or selectively dissolve inclusions.
- The morphology of the inclusions was circular on the 2D cross section and spherical for the extracted inclusions.

- The size distribution of the extracted inclusions was shifted towards larger sizes compared to the distribution observed on the polished cross section. A summary of the results showed the average 3D inclusion size was greater than the 2D size by approximately 22%.
- The shape of the inclusion size distribution for both the 2D and 3D measurements was lognormal. This suggests that 2D polished sections can be used directly to evaluate the age of an inclusion population without the need for converting the population to 3D prior to analysis.
- Application of the Schwartz-Saltykov method for converting the 2D populations to 3D resulted in an under prediction of the size distribution. The error may be due to the assumed maximum inclusion size and/or the size detection limit of the Aspex AFA analysis.
- Assuming a maximum inclusion size that was 50% greater than that observed in the 2D cross section produced a better fit between the predicted 3D distribution and the measured distribution using extracted inclusions.

ACKNOWLEDGEMENTS

The authors would like to thank the industry and faculty mentoring committee of the Peaslee Steel Manufacturing Research Center at Missouri S&T for their continuous guidance and support. Special thanks to Logan Huddleston for assisting with the steel dissolution and inclusion analysis.

REFERENCES

1. Abraham, Sunday, Justin Raines, and Rick Bodnar. "Development of an Inclusion Characterization Methodology for Improving Steel Product Cleanliness", *AIST Transactions*, Vol. 11, No. 2 (2013): 1069-1083.
2. Kaushik, P., H. Pielet, and H. Yin. "Inclusion Characterization – Tool for Measurement of Steel Cleanliness and process control: Part 1". *Ironmaking and Steelmaking* 36: 561-571.
3. E.B Pretorius, H.G. Oltmann and B.T. Schart "An Overview of Steel Cleanliness from an Industry Perspective", *AISTech* 2013: 993-1026.
4. D.L.Sahagian. and A.A. Proussevitch. "3D particle size distribution from 2D observations: stereology for natural application". *Journal of Volcanology and Geothermal Research, No. 84 (1998): 173-196*
5. Ervin E. Underwood. "Quantitative Stereology (chapter 5)" *1970*
6. T.Li, S. Ahimasaki, S.Taniguchi, and S. Narita. "Reliability of Inclusion Statistics in Steel by Stereological Methods" *ISIJ International Vol.56, No.9 (2016), 1625-1633*
7. D. Janis, R.Inoue, A.Karasev, P.G.Jonsson. "Application of Different Extraction Methods for Investigation of Nonmetallic Inclusions and Clusters in Steels and Alloys". *Advances in Material Science and Engineering, 2014.*
8. R. Inoue, S. Ueda, T.Ariyama, H.Suito. "Extraction of Nonmetallic Inclusion Particles Containing MgO from Steel*". ISIJ International Vol.51, No.12 (2011), 2050-2055*
9. M-A. Van Ende, M. Guo, E. Zinngrebe, B. Blanpain and I-H. Jung, "Evolution of Non-Metallic Inclusions in Secondary Steelmaking: Learning from Inclusion Size Distributions," *ISIJ International, Vol. 53, No. 11, 2013, pp. 1974–1982.*
10. O.Adaba, P. Kaushik, R.J. O'Malley, S.N. Lekakh, V.L. Richards, E. Mantel, R. Hall, and E. J. Ellis: "Characteristics of Spinel Inclusions Formed after Reoxidation of Calcium-Treated Aluminum-Killed Steel. *Iron & Steel Technology, July 2017, p. 38.*